
IDENTIFYING BAYESIAN OPTIMAL EXPERIMENTS FOR UNCERTAIN BIOCHEMICAL PATHWAY MODELS

Natalie M. Isenberg

Brookhaven National Laboratory
Upton NY, 11973, USA
nisenberg@bnl.gov

Susan D. Mertins

Fredrick National Laboratory for Cancer Research
Fredrick MD, 21702, USA
susan.mertins2@nih.gov

Byung-Jun Yoon

Texas A&M University
College Station TX, 77843, USA
bjyoon@tamu.edu

Kristofer Reyes

University at Buffalo
Buffalo NY, 14260, USA
kreyes3@buffalo.edu

Nathan M. Urban

Brookhaven National Laboratory
Upton NY, 11973, USA
nurban@bnl.gov

September 27, 2023

Summary

Pharmacodynamic (PD) models are mathematical models of cellular reaction networks that include drug mechanisms of action. These models are useful for studying predictive therapeutic outcomes of novel drug therapies *in silico*. However, PD models are known to possess significant uncertainty with respect to constituent parameter data, leading to uncertainty in the model predictions. Furthermore, experimental data to calibrate these models is often limited or unavailable for novel pathways. In this study, we present a Bayesian optimal experimental design approach for improving PD model prediction accuracy. We then apply our method using simulated experimental data to account for uncertainty in hypothetical laboratory measurements. This leads to a probabilistic prediction of drug performance and a quantitative measure of which prospective laboratory experiment will optimally reduce prediction uncertainty in the PD model. The methods proposed here provide a way forward for uncertainty quantification and guided experimental design for models of novel biological pathways.

Keywords Bayesian optimal experimental design · Bayesian inference · Pharmacodynamic models · Uncertainty quantification

1 Introduction

The intricate and lengthy process of discovering novel drugs stands to gain significant advantages through the application of computational methods.¹ These methods provide efficient and cost-effective avenues for exploring expansive chemical spaces, predicting molecular properties, and optimizing potential drug candidates. Dynamic models of biological systems (e.g., pharmacokinetic (PK) or pharmacodynamic (PD) models) are useful tools for studying biomolecular processes. Such models have been applied to study inter- and intra-cellular phenomena, including regulatory, metabolic, and signalling processes within human cells.^{2,3,4} These models are derived from first-principles approximations of the complex dynamics that occur *in vivo*. The utility of these biological models lies in their simplicity; tractably capturing qualitative system behaviors at the expense of prediction accuracy. Although these dynamic models are often used in preclinical drug development to determine *in vivo* drug response,⁵ they are rarely applied in drug discovery. Biological pharmacodynamic models are valuable tools in both the optimal design and validation phases of identifying novel drug candidates, making them crucial for computational drug discovery. Furthermore, regulatory agencies are beginning to accept *in silico* studies as part of the validation and testing of new medical therapies and technologies.^{6,7} This underscores a need to formalise approaches for uncertainty quantification and model improvement for pharmacodynamic models.

Uncertainty quantification is a critical analysis that is often overlooked in computational drug design, despite its relevance and available software tools.⁸ Previous studies have applied methods of uncertainty quantification to models for calibrating algorithmic parameters in automated diabetes treatment systems,⁹ a PK/PD cancer model for the antivascular endothelial growth factor in the presence of a cancer therapeutic agent,¹⁰ the calibration of dose-response relationships for the γ -H2AX assay to predict radiation exposure,¹¹ and peptide-MHC affinity prediction using a data-driven model.¹² In the aforementioned studies, experimental or clinical data was readily available for the proposed uncertainty quantification procedures. For many PD models, the scarcity of quantitative data for calibrating these models has led to significant challenges in uncertainty quantification. This limited availability of experimental data results in non-unique and/or unconstrained parameter estimations, leading to issues of nonidentifiability.¹³ Researchers have acknowledged the presence of significant parameter correlations, nonidentifiability, and parameter sloppiness in dynamic biology models, where parameters can vary over orders of magnitude without significantly affecting model output.¹⁴ Given these limitations, it is evident that incorporating uncertainty quantification to biological dynamic models, even in the absence of available data, is crucial if they are to be used for computational drug discovery and evaluation.

Optimal experimental design (OED) has been proposed as a method for improving model parameter estimates in biological pharmacodynamic models. In OED, existing measured data is used to determine what new experiment(s) should be done to best reduce parameter uncertainties.¹⁵ Several works have applied different flavors of optimal experimental design to dynamic biological models. Work done by Liepe et al.¹⁶ demonstrates OED to maximize expected information gained in a signaling pathway model featuring 6 differential equations, 4 uncertain parameters, and selecting between 5 experimental outcomes. Researchers in Bandara et al.¹⁷ showed that a sequential experimental design for a cell signaling model, coupled with fluorescence microscopy-based experimental data, was able to reduce uncertainty in some parameters, while it increased in others due to nonidentifiability. This work also provides an example of selecting optimal experiments based on an experimentally relevant metric. This approach is in opposition to the more common purely information-theoretic approach. We note that the model used in this study is relatively small, only featuring 4 differential equations, 4 uncertain rate constants, and selecting between 3 experimental possibilities. Researchers in Eriksson et al.¹⁸ utilized approximate Bayesian computation to identify approximate posterior distributions for uncertain model parameters. This work presents a larger scale problem, with 34 reactions for 25 species, 34 uncertain parameters, and 6 experimental possibilities from which to select. This approximate approach is applicable to scenarios where the data-generation distribution (likelihood function) is not available in analytic form.

In this paper, we utilize methods from Bayesian optimal experimental design using exact Bayesian inference and Hamiltonian Monte Carlo (HMC) to recommend experiments for mechanistic model improvement. Our focus is on a dynamic model of programmed cell death, i.e., *apoptosis*. This model predicts synthetic lethality in cancer in the presence of a *PARP1* inhibitor. Therefore, when we refer to selecting an optimal *experimental design*, we mean “which species should we measure from a *PARP1*-inhibited cell experiment to improve confidence in simulated lethality predictions of a given inhibitor?” Our goal is to first understand the impact of parameter uncertainty on the predictive reliability of this model. Then, the aim is to recommend experimental measurements that can be done in the lab to maximize confidence in simulated lethality predictions. To do this, we conduct parameter inference using HMC for large volumes of data generated from simulated experiments. This way, we can determine which experimental data, in expectation, would most reduce uncertainty in modeled drug performance predictions. Such an approach provides researchers with a quantitative method for linking physical experiment design to model improvement in the absence of existing data.

It is important to note that while our optimal experimental design study is conducted with simulated experimental data, and the results are thus subject to our modeling assumptions, the dynamic model underpinning our analysis contains biologically relevant and measurable parameters, thus offering insights that can guide future experimental endeavors. Furthermore, the framework we lay out here is general and applicable to any relevant biological modeling setting where experimental data is obtainable.

Formally, the contributions of this work are threefold: (1) Applying Bayesian optimal experimental design and high-performance computing (HPC) to a large-scale coupled ODE system of 23 equations and with 11 uncertain parameters and choosing between 5 experimental designs — the largest PD system considered thus far in a fully Bayesian OED framework of which the authors are aware; (2) Proposing novel decision-relevant metrics for quantifying the uncertainty in therapeutic performance of novel inhibitor drugs at a given concentration (IC_{50}); and (3) Identifying optimal experiments that minimize the uncertainty in therapeutic performance (i.e., simulated lethality) as a function of the inhibitor dosage of interest.

As we will show, there is preference for measuring activated caspases at low IC_{50} to reduce uncertainty in the probability of cell death. At larger IC_{50} , our results show that this uncertainty is maximally reduced by collecting data the

mRNA-Bax concentrations. Therefore, we conclude that the decision as to which species to experimentally measure must be selected by considering trade-offs between the predicted BOED objectives and the inhibitor viability *in vitro*. The approach and results presented here thus bridge model-guided optimal design with uncertainty quantification, advancing drug discovery through uncertainty-aware decision-making.

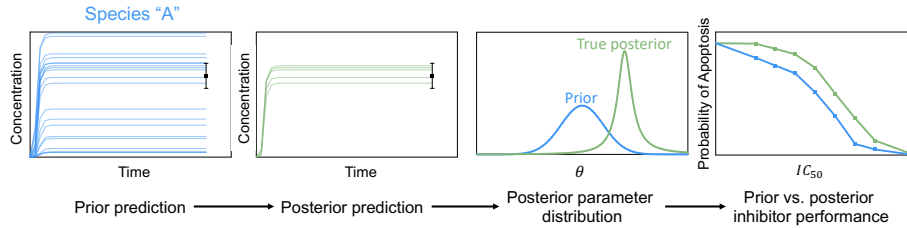
2 Methods

The problem addressed in this work is to understand the impact of model parameter uncertainty on the predictive capacity of the PD model for *PARP1*-inhibited cellular apoptosis; a representative model for cancer drug evaluation. And given the effects of uncertainty and lack of experimental data, we wish reestablish a predictive model by recommending measurements that can be made in the lab to better constrain the model parameters.

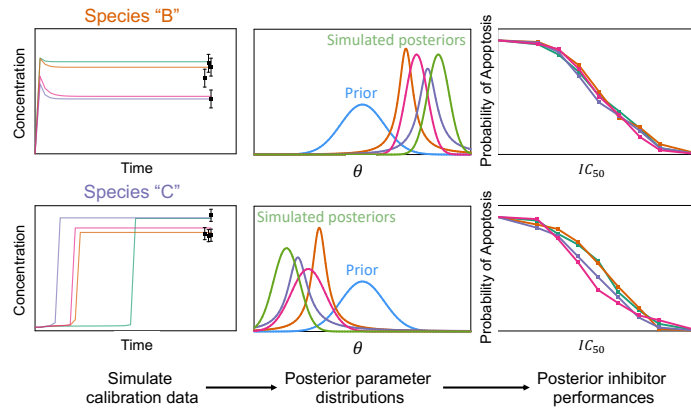
The workflow to achieve the stated goals is as follows:

1. Acquire many (synthetic) experimental measurements for each prospective measurable species in the model
2. Construct *prior probability distributions* (i.e., beliefs regarding model parameter distributions in the absence of data)
3. Conduct parameter estimation via Bayesian inference using the model, data, and prior probabilities for each prospective experiment and over multiple data samples
4. Compute expected drug performance predicted by the model given *posterior probability distributions* (i.e., updated parameter distribution beliefs after incorporating data)
5. Rank and recommend experiments based on a metric that quantifies reliability in model predictions.

A graphical depiction comparing traditional parameter calibration to the proposed approach using simulated experimental data is shown in Figure 1.



(a) Model parameter calibration with real data.



(b) Model parameter calibration with simulated experimental data.

Figure 1: Workflow for Bayesian parameter calibration using (a) real, measured data and (b) experimental data simulated from the model.

Traditional model parameter calibration via Bayesian inference is shown in Figure 1a. The model-derived prior predictive distribution of concentration profiles for **Species "A"** is constrained by experimental data (in **black**). This leads to an updated probability density function for the model parameters θ referred to as the *posterior distribution*. The posterior distribution is then used to quantify inhibitor performance via probability of achieving apoptosis in simulation across an array of IC_{50} values. We can then compare the expected inhibitor drug performance between the prior and posterior uncertainty. More accurate predictions by the posterior are thus expected because real data was used to update the model.

The methodology utilized in the present work is presented in Figure 1b. Here, we do not have access to real, measured data to constrain our model. However, we can use the PD model and an expert-derived error model to generate an ensemble of simulated experimental data. In simulating and calibrating to a large volume of simulated experimental data, we account for uncertainty in what *could* be measured in reality (in **black**). This then leads to an ensemble of posterior distribution predictions for the parameters θ . We obtain ensembles of posterior parameter distributions for several potential measurable species in the model (e.g., **Species "B"** and **Species "C"**). From these, we can compute an ensemble of inhibitor performances as measured by probability of apoptosis across a range of IC_{50} values. This implies a distribution on expected inhibitor performances as predicted by "measuring" different species and using the simulated measurements for calibration. By comparing the distributions in expected inhibitor performance across different measured species, we can identify which experiment is "optimal" by selecting the one that leads to the greatest reduction in uncertainty.

2.1 Mathematical Model

The general form of a pharmacodynamic model is shown in Eqn. 1, which represents a set of coupled ordinary differential equations.

$$\begin{aligned}\dot{y}(t) &= f(y(t); u, \kappa) \\ y(t_0) &= y_0\end{aligned}\tag{1}$$

In the rate-based modeling framework used here, variables $y(t) \in \mathbb{R}^n$ are state variables representing the time-varying concentrations of the n chemical species of interest within the cell signalling pathway. The parameters $\kappa \in \mathbb{R}^m$ are the parameter data, which includes the kinetic rate constants for the reaction network. Initial concentrations of species are those at t_0 , specified by the value of the vector $y_0 \in \mathbb{R}^n$. The system parameters and time-varying species concentrations are related by the functions $f: \mathbb{R}^n \rightarrow \mathbb{R}$, indexed by $\forall i \in \{1, \dots, n\}$. Also, we separate the input parameters in Equation 1 into two vectors: u , the control variables, and κ the uncertain model parameters. The pre-specified input parameters u are any experimental controls set *a priori*. In the model considered here, this is the half maximal inhibitory concentration (IC_{50}) for a novel *PARP1* inhibitor molecule. IC_{50} is a commonly used metric in experimental biology for quantifying a molecule's ability to inhibit a specific biological function.

2.2 Bayesian Optimal Experimental Design

Bayesian optimal experimental design is a statistical framework that aims to identify the most informative experimental conditions or measurements to improve parameter estimation and model predictions in the presence of uncertainty.^{19,20} It involves iteratively selecting experiments^{21,22} that maximize the expected information gain or other objectives, such as mean objective cost of uncertainty,^{23,24} given prior knowledge, model uncertainty, and the available resources. The goal is to strategically design experiments that provide the most valuable information via uncertainty reduction in the calibrated model predictions.

In our application, we want to identify an experimental design ξ (i.e., a specific species we can measure from the cell in the presence of a *PARP1* inhibitor) from the set of feasible designs, Ξ , which optimizes information gain regarding uncertain parameters, θ , given the outcome of that experiment, y . Let us denote the set of all uncertain parameters within the ODE system, including initial conditions and rate constants, as the set Θ . For tractability reasons, we may choose to only consider a subset of the parameters which are deemed most significant via global sensitivity analysis and refer to the vector of key, significant parameters as $\theta \in \Theta$. We also denote the vector of experimental designs being considered as $\xi \in \mathcal{X} \subset \Xi$, and $|\mathcal{X}| = N_\xi$ is the number of design decisions to choose from in optimization. Here, the individual experiments represent a species to measure in an experiment representing the process modeled in the *PARP1*-inhibited cell apoptosis PD model. We assume prior distributions on the uncertain parameters $p(\theta)$, and a likelihood of the data conditional on the parameters and controls variables, $p(y|\theta, \xi, u)$. For a general objective function of interest, $\mathcal{J}(\xi; u)$, where ξ are the decision variables and u inputs to Equation 1, the Bayesian optimal experimental design task is described by Equation 2.

$$\xi^* = \arg \max_{\xi \in \Xi} \mathcal{J}(\xi; u) \quad (2)$$

Traditionally, this objective \mathcal{J} is the expected information gain (EIG), a quantitative measure of entropy reduction between the prior and posterior probability distributions of θ .^{25,26} Under such a formulation, the objective function becomes a nested expectation computation under the marginal distribution of experimental outcomes. The posterior distributions are often then estimated using a Markov Chain Monte Carlo (MCMC) algorithm to compute the information gained. For this application, we are not interested in optimal experiments which simply minimize relative entropy in the prior and posterior distributions in θ , as is the standard practice in BOED. Instead, we wish to select optimal experimental designs that minimize uncertainty in lethality predictions made by the ODE model under different inhibitor drug IC_{50} , i.e., different $u \in \mathcal{U}$. In this model setting, lethality (i.e., probability of cell apoptosis) can be viewed as a probabilistic analog to the traditional dose-response curve and is defined in Equation 3.

To that end, we devise two metrics for quantifying uncertainty in cell lethality predictions at different IC_{50} values. The first is the uncertainty in the probability of triggering cell apoptosis at a given IC_{50} , represented as $\sigma_{apop}(u)$. A graphical representation of $\sigma_{apop}(u)$ across IC_{50} is shown in Figure 2a. This quantity defines a characteristic height of the distribution of the lethality curve predictions at a specific IC_{50} of interest. Smaller σ_{apop} values thus imply that there is higher confidence in the PD model predictions at the IC_{50} they are computed at. One may choose to only consider the σ_{apop} at very small IC_{50} , since we are interested in drug molecules which are most effective at low doses.

The second metric provides a quantification of the uncertainty in the inhibitor drug dosage (i.e., IC_{50}) that achieves a given probability of triggering cell apoptosis, and is represented as $\sigma_{IC_{50}}(\mathbb{T})$. A graphical representation of $\sigma_{IC_{50}}(\mathbb{T})$ across IC_{50} and for $\mathbb{T} = 0.75$ is shown in Figure 2b. This metric defines a characteristic width of the lethality distribution at a target probability of triggering cell death, $\mathbb{T} \in [0, 1]$. A smaller $\sigma_{IC_{50}}$ value at a given \mathbb{T} implies higher confidence in which IC_{50} value achieves a given probability of killing the cell. More detail on these metrics is discussed in Appendix 6.3. In addition, we discuss the multi-objective treatment of these two metrics, and the sensitivity of the optimal recommended experiment to that treatment, in Section 4.

3 Application

We consider a dynamic *PARP1*-inhibited cell apoptosis models for both wild-type human cells published in.²⁷ We note that this pathway can be found in some tumorous cells, as well. Thus, for the present study, the process that this model represents is the inhibition of *PARP1* as a therapy for cancer. By applying an inhibitor via a specified IC_{50} , inhibition of *PARP1* halts the DNA strand break repair process, reducing damage repair pathways and potentially leading to cell apoptosis. Further information on the model and the complete system of differential equations is available in the Equation S12.

The model consists of a set of 23 ordinary differential equations (ODE) wherein a subset of the 27 rate constant parameters are considered uncertain. This model takes as inputs (1) an IC_{50} value and (2) initial conditions and (3) kinetic parameter values. In the present study, we only consider output at a specific time point, (i.e., the final time point) when performing inference. This means that the likelihood we supply for the data follows a Normal distribution in the model prediction at $t = \tau$, where τ is the time limit for the numerical integrator used to solve the ODE system at a given IC_{50} , and with a known σ that is computed with a 10% error relative to the model prediction. Information for the uncertain parameters considered in this study was first elicited from expert understanding of the system and relevant sources. Nominal parameter values and confidence interval information is shown in Table S1. Details regarding the construction of all prior distributions on uncertain parameters considered in the present study are provided in Table S2. In addition, because experimental data for species concentrations within a single cell undergoing *PARP1*-inhibited apoptosis are not readily available, we utilize simulated experimental data for our study that is generated via the procedure described in Appendix Section 6.1.

3.1 Objective function specification

As noted previously, the quantity-of-interest in assessing the performance of *PARP1* inhibitor is the predicted lethality. The predicted lethalties are then used to compute our uncertainty metrics or objective functions, $\sigma_{apop}(u)$ and $\sigma_{IC_{50}}(\mathbb{T})$. Here, we specify the method for computing lethality, i.e., probability of triggering cell death. It has been shown that a activated caspase molecule count in the cell above a threshold of 1,000 is sufficient to trigger cell apoptosis.¹⁶ Therefore, we can compute whether or not cell apoptosis has been irreversibly triggered by the introduction of a *PARP1* inhibitor by computing $y_k^{max} := \max_{t \in [1, \dots, \tau]} y_k(t)$ where $k = \text{Casp-act}$. Thus, lethality, or $P(\text{apoptosis})$ can be computed by sampling

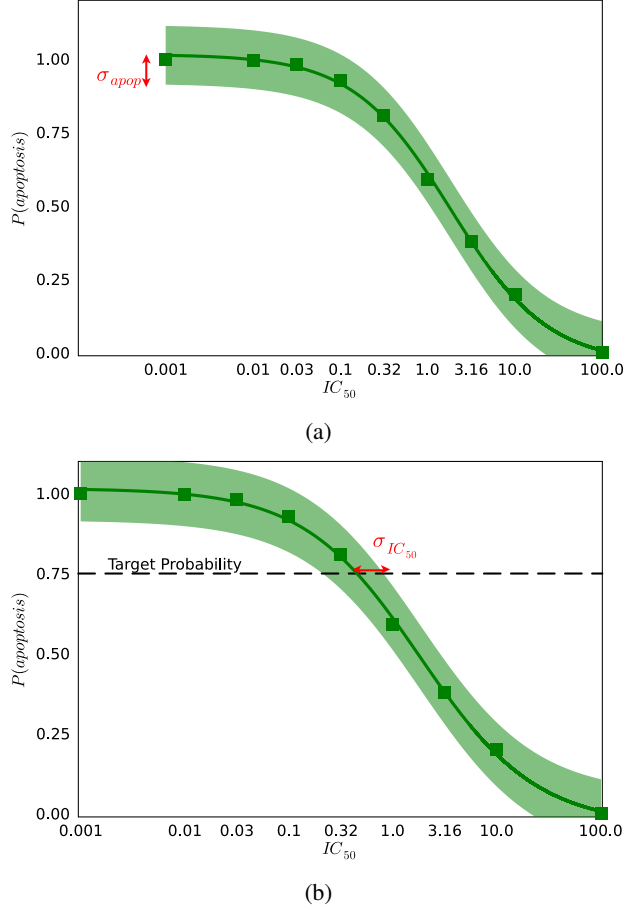


Figure 2: Graphical depictions of uncertainty metrics for probabilistic lethality curves in (a) $\sigma_{apop}(u)$ at $u = 0.001$ and (b) $\sigma_{IC_{50}}(\mathbb{T})$ at target probability threshold $\mathbb{T} = 0.75$. The shaded green region represents a distribution of *lethality curves* that is computed from an ensemble of posterior distributions in the uncertain parameters θ . The mean of this distribution in lethality curves is shown in the square data points.

the prior (posterior) probability distributions of the uncertain parameters, $\theta^i \sim p(\theta) \forall i \in [1, \dots, N_s]$, specifying a value for IC_{50} , and integrating the system of ODEs. Given the ensemble of N_s maximum-caspase concentrations, $P(\text{apoptosis})$ can be calculated as shown in Equation 3.

$$P(\text{apoptosis}) := \frac{1}{N_s} \sum_{i=1}^{N_s} \mathbb{1}_{y_{Casp,i}^{max} \geq 1000} \quad (3)$$

Here, N_s is the Monte Carlo sample count. When computed at all IC_{50} of interest, we retrieve a vector of $P(\text{apoptosis}|u)$ predictions $\forall u \in \mathcal{U}$, producing a *lethality curve* for a given posterior parameter estimate.

3.2 Incorporating biological constraints

In addition to the expert-elicited prior probability information in Table S1, there is other biologically and therapeutically relevant information that we can incorporate into Bayesian parameter estimation to further constrain our posterior predictions. First, we know that for *PARP1* inhibitor drugs with sufficiently high IC_{50} values (i.e., low efficacy), we expect the repair signal from *PARP1* to win out over the programmed cell death induced by p53. This means that at high IC_{50} , the DNA double strand break will be repaired and the cell will live. We also know the opposite to be true: for low IC_{50} , programmed cell death will be induced and the cell will die. In mathematical terms, we can say:

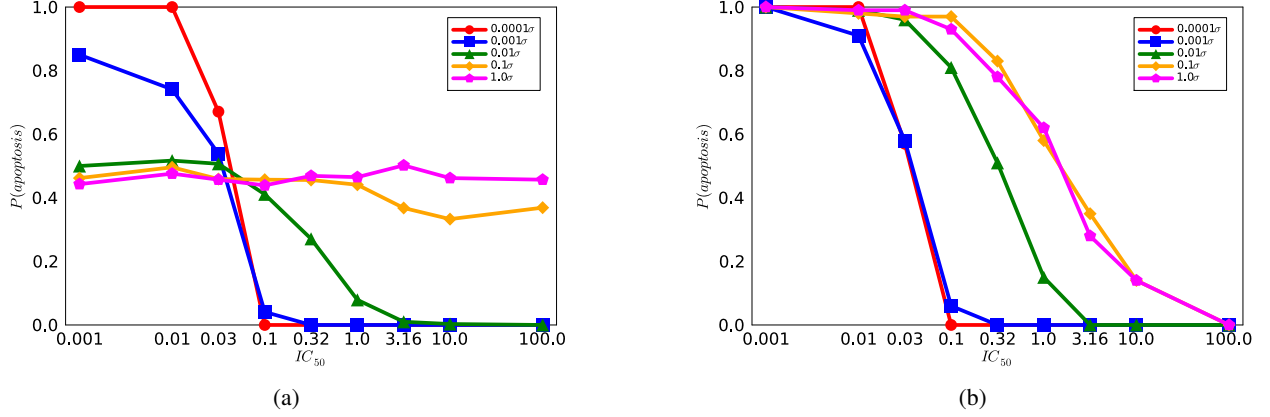


Figure 3: The probability of cell death $P(\text{apoptosis})$ plotted against IC_{50} for different multiplicative factors of the standard deviation σ in the prior distributions (a) without and (b) with applying the constraints in Equation 4.

$$P(\text{apoptosis}) = \begin{cases} 0, & \text{if } IC_{50} \geq 100 \\ 1, & \text{if } IC_{50} \leq 0.001 \\ \text{Equation 3} & \text{otherwise} \end{cases} \quad (4)$$

This prior knowledge regarding the effect of a drug on our quantity of interest does not directly translate to knowledge regarding the uncertain model parameters. However, because the quantity of interest is computed directly from an output of the model (i.e., concentration of activated caspases) we can still include this prior knowledge in Bayesian inference in three equivalent ways: in the likelihood, the prior, or through *post facto* filtering of the estimated posterior chain. For the present application, we choose the posterior filtering approach due to numerical challenges in the HMC sampling algorithm used to estimate the posterior distribution.

The posterior filtering approach used involves sampling a larger chain (in this study, 50,000 samples) for each simulated experimental data point. If a given parameter sample in the posterior chain leads to the violation of the constraints in Equation 4 when specified in the forward simulation model under the nominal IC_{50} (i.e., Talazoparib, see Appendix Section 6.1), that sample is removed from the chain.

4 Results and Discussion

In this section, we provide the key findings of our study applying Bayesian optimal experimental design to the *PARP1*-inhibited cell apoptosis model. First, we conduct a prior sensitivity analysis, follow by posterior estimation and computation of our optimal experimental design objectives.

4.1 Prior Sensitivity

We conducted a prior sensitivity analysis computed for a quantity of interest, $P(\text{apoptosis})$. The purpose of this study is to understand how much reduction in uncertainty is required to achieve desired lethality curve predictions. The result of this study is shown in Figure 3. Here, the $P(\text{apoptosis})$ is computed by (1) drawing 1,000 random samples from prior probability distributions for each uncertain parameter, then (2) solving the model in Equation S12 at those parameter sample values and (3) computing $P(\text{apoptosis})$ via Equation 3 for all $IC_{50} = [0.001, 0.01, 0.032, 0.1, 0.32, 1.0, 3.2, 10.0, 100.0]$. To determine the model sensitivity against the priors, we scale σ for each parameter by a multiplicative factor to narrow the support of the prior distribution around its nominal mean. In Figure 3a, we neglect our prior constraints and just solve the model under the unconstrained prior samples. Under these conditions, we see that given the nominal prior uncertainty (i.e., 1.0σ), the effect of IC_{50} on lethality vanishes (i.e., it is a more-or-less flat line). From the results, it appears that the model requires *at minimum* a reduction in prior uncertainty of two orders of magnitude (i.e., 0.01σ) before a predictive model is restored via sigmoidal curvature in the prior lethality curve. This implies that achieving a reduction in uncertainty spanning two orders of magnitude across all uncertain parameters is imperative to differentiate therapeutic performance between different inhibitors using the PD model.

In Figure 3b, we conduct the same sensitivity analysis while also applying the constraints in Equation 4 to restrict the model-predicted lethality values using biological insights. Under these conditions, we obtain lethality curve predictions that have the desired sigmoidal shape, showing low therapeutic performance at large IC_{50} and high therapeutic performance at small IC_{50} . However, it is also evident that significant reduction in parameter uncertainty (0.0001σ) is required to achieve apoptotic switch behavior at low IC_{50} .¹⁶

It is worth noting that this sensitivity analysis involved altering all prior σ values by the same amount, and the existence of parameter correlations could potentially yield alternative outcomes in terms of the necessary uncertainty reduction. However, these results underscores the need for substantial reduction in parameter uncertainty in PD models to re-establish predictive ability.

4.2 Posterior Estimation

We estimate posterior probability distributions for the uncertain parameters using the proposed Bayesian optimal experimental design approach. Details regarding the underlying algorithm are provided in Appendix Section 6.2. The summary statistics for (1) mean posterior parameter estimates, (2) effective sample size per parameter, and (3) filtered chain length are shown in Table S7–S16. The filtering procedure leads to non-uniform posterior chain lengths and lower effective sample sizes, as shown in the summary statistics. We note that only approximately 1% of samples in the posterior chains pass the constraints enforced via Equation 4. This is indicative of a known challenge in applying feasibility constraints after sampling: that the vast majority of the parameter space explored is ultimately infeasible, even for sufficiently large chains. Therefore, in future work, we aim to explore methods such as Bayesian constraint relaxation²⁸ to enforce relaxed constraints on our probabilistic model while maintaining numerical stability in standard Hamiltonian Monte Carlo sampling algorithms. Still, the average ESS per parameter is still close to the average chain length for each species, implying a high number of non-correlated samples in the posterior chains we computed. Additionally, we note that the assumption of Log-Normal prior probability distributions for all the model parameters in Table S1 is an assumption with ramifications on the final derived posterior distributions.

4.3 Value of Information Estimation

The ensemble of predicted lethality curves for each species in Table S3 are shown in Figure 4. It is clear from the plots that certain species induce less spread in lethality predictions across IC_{50} (e.g., mRNA-Bax) while other exhibit more variability (e.g., Casp-pro). To quantitatively understand these trends, we compute the values of $\sigma_{apop}(u)$ and $\sigma_{IC_{50}}(\mathbb{T})$. The plots in Figures 5a-5b show how these uncertainty metrics evolve over u and \mathbb{T} , respectively. Tabulated results are available in Tables S4 and S5.

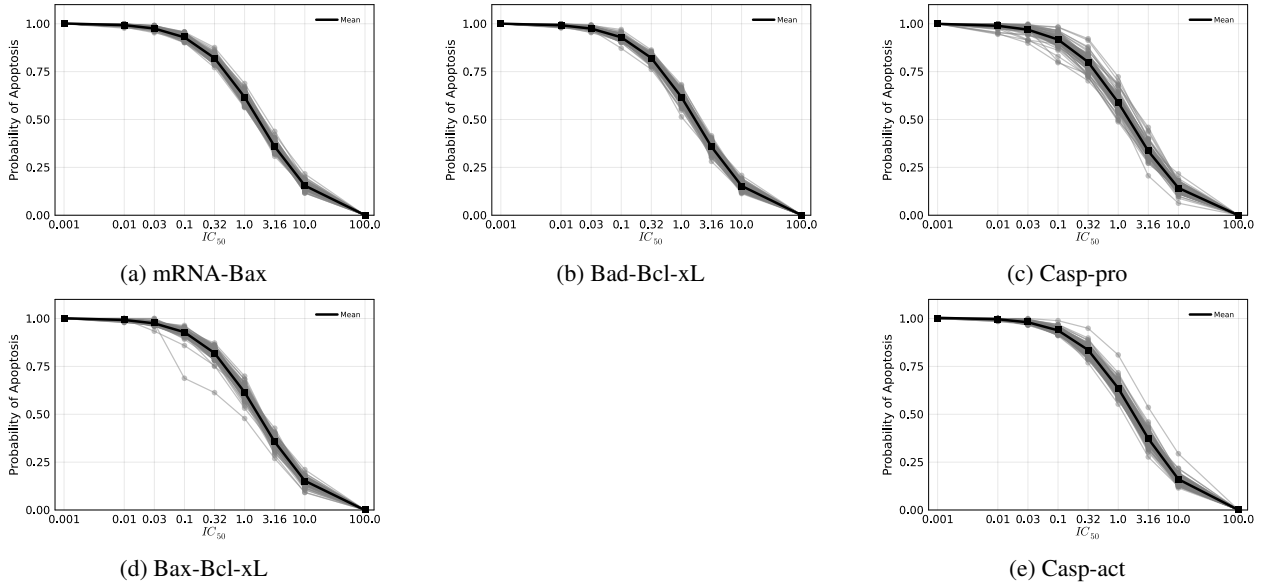


Figure 4: Ensemble of lethality curves predicted for each measurable species considered at different IC_{50} values. Each individual curve represents a different lethality prediction obtained from a single synthetic experimental measurement. The mean over all 100 measurements is shown in black.

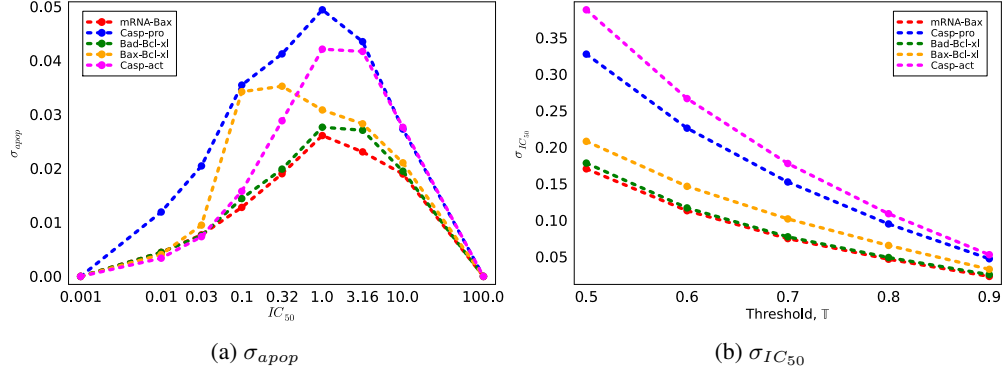


Figure 5: Uncertainty metrics for synthetic lethality computed at different IC_{50} using posterior distributions inferred using concentration data for the measurable species considered.

It is seen in Figure 5a that there is a regime at small IC_{50} (which is the regime with the greatest therapeutic viability) wherein the minimizer of σ_{apop} changes. In particular, at $IC_{50} = 0.01$ and $IC_{50} = 0.03$, the ξ which minimizes the σ_{apop} objective is Casp-act. At $IC_{50} > 0.03$, the minimizer becomes mRNA-Bax for the rest of the IC_{50} range considered. This can also be seen in Table S4, where the minimum value of σ_{apop} in each column (i.e., for each IC_{50}) is demarcated with an $*$.

When considering the σ_{apop} objective alone, and when only placing significance in reducing uncertainty at low IC_{50} , the optimal decision $\xi^* = \text{Casp-act}$. At $IC_{50} = 0.01$, the potential reduction in uncertainty in $P(\text{apoptosis})$ under experimental designs (i.e., measurements) $\xi^* = \text{Casp-act}$ is 24% when compared to Bad-Bcl-xL, the species with the highest σ_{apop} (0.01). We note again that reduction in σ_{apop} directly translates to a reduction in the uncertainty regarding the predicted $P(\text{apoptosis})$ for a given inhibitor (i.e., at a given IC_{50}). This is analogous to reducing uncertainty in a given inhibitor drug’s expected performance. In summary, this result implies that it is optimal to acquire and calibrate to experimental data regarding Casp-act concentrations if we wish to maximize confidence in the expected lethalities of inhibitors with with low IC_{50} .

In the case of $\sigma_{IC_{50}}$, as shown in Figure 5b, the trend of which ξ minimizes the objective remains consistent across threshold values $\mathbb{T} = [0.5, 0.6, 0.7, 0.8, 0.9]$. Thus, when considering the $\sigma_{IC_{50}}$ objective alone, and for any threshold, the optimal $\xi^* = \text{mRNA-Bax}$. We note that reduction in $\sigma_{IC_{50}}$ directly translates to a reduction in the uncertainty regarding which IC_{50} achieves the target $P(\text{apoptosis})$ threshold, \mathbb{T} . This is analogous to reducing uncertainty in a which inhibitor drug achieves the desired expected performance. For a potent inhibitor with $\mathbb{T} = 0.9$, selecting the optimal experimental design $\xi^* = \text{mRNA-Bax}$ over Casp-act (i.e., the species with the highest $\sigma_{IC_{50}}$ (0.9)) results in a substantial 57% reduction in uncertainty regarding the specific IC_{50} associated with achieving this cell death probability. In summary, this result implies that it is optimal to acquire and calibrate to experimental data regarding mRNA-Bax concentrations if we wish to maximize model prediction confidence in which inhibitor dosage achieves a given expected lethality.

When combining these two metrics to determine an optimal experimental design (i.e., which protein to measure in the lab to reduce uncertainty in lethality curve predictions) we provide an optimal design ξ^* against the following objectives: (1) $\sigma_{IC_{50}}$ at a threshold of 0.90, (2) σ_{apop} at $IC_{50} = 0.01$, and (3) weighted averages of both. In the case of the weighted averages, we take the objective to be defined as: $w_1\sigma_{IC_{50}} + w_2\sigma_{apop}$ wherein $w_1 + w_2 = 1$. For the purposes of illustrating the sensitivity of the combined objective to the selection of weights w_1, w_2 , we show this weighted average objective under $w_1 = [0.01, 0.1]$. These results are tabulated in Table S6. The results of the weighted average show that at $w_1 = 0.01$, Casp-act is optimal, while at $w_1 = 0.1$, mRNA-Bax is preferred. Although the weights used here are arbitrary, domain knowledge should be integrated in the assignment of weights, leading to optimal experiments that align with what is understood regarding the underlying biological pathways.

In each of the objectives considered, activated caspase or Bax mRNA are identified as the optimal experimental measurements that could maximally reduce model prediction uncertainty if used in calibration. Here, we provide some insight as to why this may be the case given the present study. A possible explanation for the switch from $\xi^* = \text{Casp-act}$ to $\xi^* = \text{mRNA-Bax}$ at low to intermediate IC_{50} may be because of the time dynamics. If a higher IC_{50} is needed to kill a cancer cell via apoptosis, then measuring a species that represent the precursor steps to triggering apoptosis may more informative than the activated caspase itself. It is also possible that mRNA-Bax performs best across a wider range of drug dosages because it is more proximal to the mechanism of action. Once *PARP* is inhibited, only a few reactions are needed to trigger mRNA-Bax formation, and ultimately, the activation of caspase.

These differing outcomes across the different experimental design objectives underscore the essential role of biological insights in differentiating among optimal experimental designs.

5 Conclusions

In this work, we utilized a realistic PD model for *PARP1*-inhibited cell apoptosis in a model-guided optimal experimental design workflow to reduce uncertainty in the performance of cancer drug candidates. We first showed that, under prior uncertainty, the ability for the model to discriminate between *PARP1*-inhibitor therapeutic performance disappears. Through extensive simulations and Bayesian inference, we have demonstrated the potential of our methodology to reduce parameter uncertainties and reestablish a discriminatory PD model for drug discovery. Additionally, our exploration of the *PARP1* inhibited cell apoptosis model has yielded novel insights into species-specific dependencies with *PARP1* inhibitor IC_{50} , informing optimal measurement choices. Introducing therapeutic performance metrics based on the half maximal inhibitory concentration (IC_{50}), we provide a comprehensive evaluation of drug efficacy under parameter uncertainty. Specifically, we identified optimal experiments under three distinct objectives: (1) $\sigma_{IC_{50}}$ at a threshold of 0.90, (2) σ_{apop} at $IC_{50}=0.01$, and (3) a weighted average of both metrics. At low IC_{50} , our results indicate that measuring activated caspases is optimal, with the potential to significantly reduce uncertainty in model-predicted cell death probability. And at high IC_{50} , Bax mRNA emerges as the favored contender for experimental measurement. We note that our algorithmic approach, which includes collecting a large number of posterior samples and then rejecting parameter samples that violate biological constraints, leads to a majority of samples being rejected. Therefore, in future work, we will explore alternatives for enforcing biological constraints in Bayesian inference, such as relaxed constraints in the data likelihood. Additionally, we would like to identify lab experiments that can be conducted to acquire data which is compatible with our model so that we can validate the results of our OED and further constrain the model parameters. In summary, our combined metric-based approach not only elucidates the importance of tailored species measurements to minimize uncertainty in lethality curve predictions but also introduces a flexible framework for optimal experimental design using novel biological pathway models. Thus, our contributions bridge the critical gap between model-guided optimal design and uncertainty quantification, advancing the realm of computational drug discovery.

6 Appendix

6.1 Simulated Experimental Data

Simulated experimental data was generated for each of the N_{ξ} observable proteins by taking random parameter samples from their respective prior predictive distributions (see Figure S8) and modifying these samples via a relative error of 10% across all parameters. The value of 10% was selected as it is the typical standard deviations found in experimental measurements in the laboratory. First, N_d random draws from the parameter prior distributions are made independently for each uncertain parameter, i.e. $\theta_i^{sim} \sim p(\theta) \quad \forall i = [1, \dots, N_d]$. Next, the θ_i^{sim} are used to solve the forward model in Equation S6 at an $IC_{50}=0.005083 \mu M$, which is the measured IC_{50} for WT cells under the *PARP1*-inhibitor Talazoparib, as shown in Figure 6. This generates a “true” y .

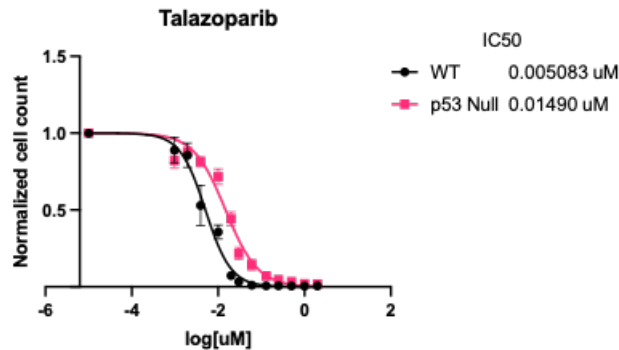


Figure 6: The HCT116 dose response curves. Details on the study can be found in.²⁷

The noisy $y_{k,i}^{sim} \quad \forall k = [1, \dots, N_{\xi}], \forall i = [1, \dots, N_d]$ used in inference in this work is generated by applying a multiplicative error ϵ , where we assume that the error is log-normally distributed. Therefore,

$$y_{k,i}^{sim} = y_{k,i}\epsilon, \quad \log(\epsilon) \sim \mathcal{N}(0, \sigma^2) \quad \forall k = [1, \dots, N_\xi], \forall i = [1, \dots, N_d]$$

Where the standard deviation σ is 0.1 for all species k . It follows that:

$$\begin{aligned} \log(y_{k,i}^{sim}) &= \log(y_{k,i}) + \log(\epsilon) \\ y_{k,i}^{sim} &\sim \exp(\log(y_{k,i}) + \log(\epsilon)), \end{aligned}$$

$\forall k = [1, \dots, N_\xi], \forall i = [1, \dots, N_d]$. To avoid numerical issues at 0 concentrations (i.e., $y_{k,i} = 0$), we employ a parameter a defined such that $a = b - \min\{y_{k,i}\}$, where b is a small tolerance (in this study, $b = 0.001$). Leading to the final form of our simulated experimental data as:

$$y^{sim} \sim \exp(\log(y + a) + \log(\epsilon)), \quad \log(\epsilon) \sim \mathcal{N}(0, \sigma^2)$$

6.2 Algorithmic approach

The workflow diagram depicted in Figure 7 outlines the systematic procedure employed for conducting Bayesian Optimal Experimental Design (BOED) within the context of the *PARP1*-inhibited cell apoptosis model.

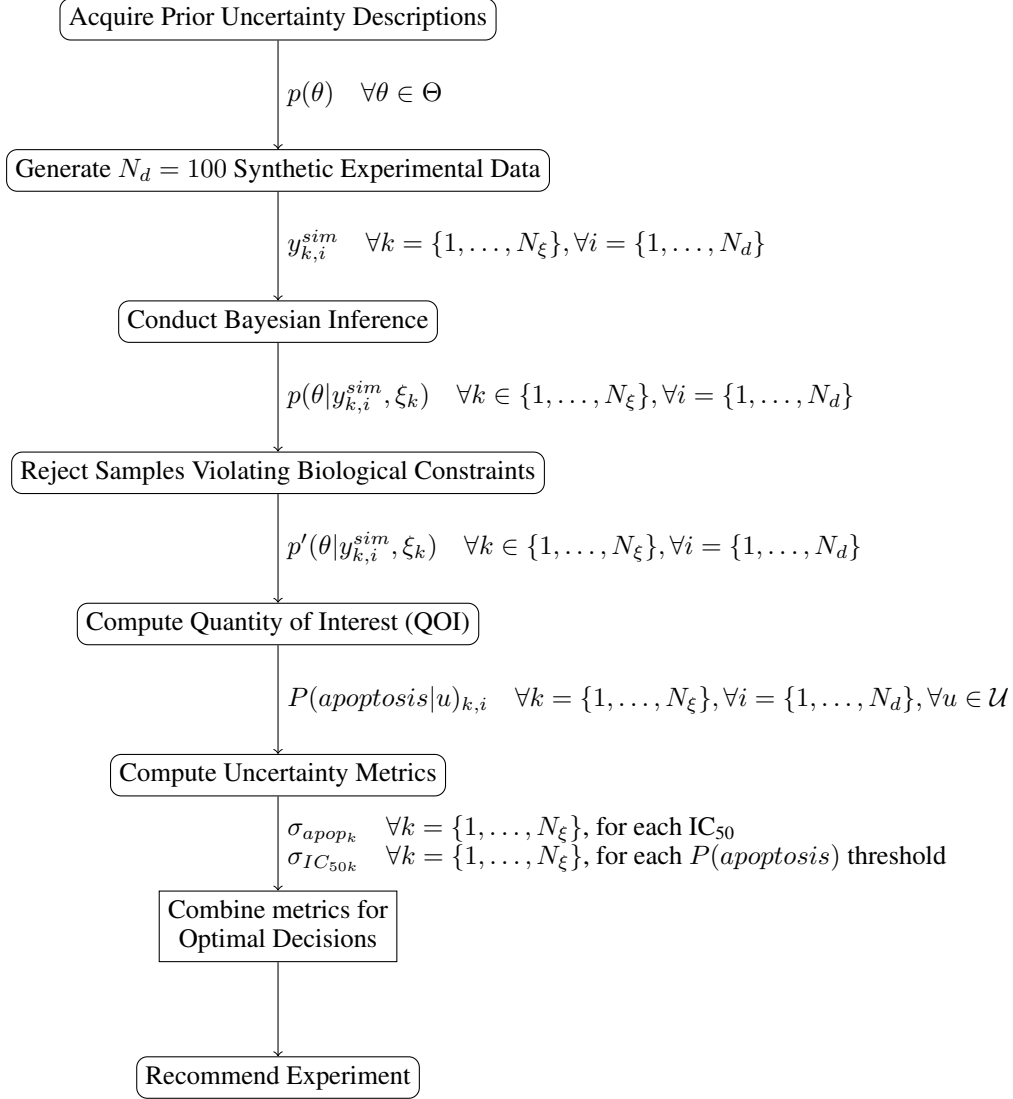


Figure 7: Workflow utilized for Bayesian experimental design for the *PARP1*-inhibited cell apoptosis model.

The process begins by specifying prior uncertainty descriptions for the key model parameters ($p(\theta) \quad \forall \theta \in \Theta$) determined by global sensitivity analysis results presented in.²⁷ This subset is shown in Table S1. Next, synthetic experimental data ($y_{k,i}^{sim}$) are generated for each experimental design (indexed by $k = \{1, \dots, N_\xi\}$) under consideration, as listed in Table S3, and for $i = \{1, \dots, N_d\}$ samples from the prior distributions and a known error model (see Table S7). We note that we select the experimental designs listed in Table S3 because these species exhibited high prior predictive uncertainty, as seen in Figure S8. These synthesized data are used to constrain the uncertain model parameters via Bayesian Inference, where the posterior parameter probability distributions ($p(\theta|y_{k,i}^{sim}, \xi_k)$) are estimated using a HMC algorithm (i.e., a type of MCMC algorithm for sampling from an unknown distribution) for each $k = \{1, \dots, N_\xi\}$ and for each datum $i = \{1, \dots, N_d\}$. Next, constraints based on biological feasibility are then applied to reject samples in the Markov chains that violate the expected behavior of the cell under extreme *PARP1* inhibitor dosages. This leads to modified posterior estimates ($p'(\theta|y_{k,i}^{sim}, \xi_k)$). These posterior distributions are then utilized to compute the Quantity of Interest (QOI), specifically the probability of cell apoptosis ($P(apoptosis|u)$), which is assessed for various inhibitor IC_{50} values ($u \in \mathcal{U}$). These QOI values serve as the basis for computing the uncertainty metrics: $\sigma_{apop}(u)$ and $\sigma_{IC_{50k}}(\mathbb{T})$ for each experimental design. Finally, the uncertainty metrics are combined to make optimal experimental decisions, thereby providing recommendations for the most effective experimental designs. This comprehensive workflow guides the process of leveraging BOED to enhance our understanding of how we can optimally reduce uncertainty in the model predictions made by the *PARP1*-inhibited cell apoptosis model under different drug dosage conditions.

6.3 Uncertainty Metrics

The calculated lethality serves as the basis for deriving our fundamental experimental design objectives: the $\sigma_{IC_{50}}(\mathbb{T})$ and $\sigma_{apop}(u)$ uncertainty metrics. These metrics offer a quantifiable means of assessing the reduction in uncertainty associated with the various experimental designs, ξ .

The $\sigma_{IC_{50}}(\mathbb{T})$ metric is determined by fitting a 4-parameter sigmoidal curve, specifically the form $P(apoptosis|IC_{50})_i = d_i + \frac{a_i - d_i}{1 + (\frac{IC_{50}}{c_i})^{b_i}}$, to the computed $P(apoptosis|u)_i$ values for each IC_{50} value and for each $i \in [1, \dots, N_d]$. Subsequently, the intersection points of the sigmoidal fits with pre-specified $P(apoptosis)$ thresholds (e.g., $\mathbb{T} = [0.5, 0.6, 0.7, 0.8, 0.9]$) determine the associated IC_{50} values. The $\sigma_{IC_{50}}(\mathbb{T})$ metric is then defined as the standard deviation over IC_{50} values at which the sigmoidal fits intersect the threshold.

The σ_{apop} metric is computed by taking the standard deviation over all predicted probabilities of apoptosis at a given IC_{50} , i.e., $P(apoptosis|u)_i$, $\forall i = [1, \dots, N_d], \forall u \in \mathcal{U}$. This is defined in Equation 5, where $\bar{P}(apoptosis|u)$ is the arithmetic mean of the predicted probabilities of cell death at the specified inhibitor IC_{50} , or u .

$$\sigma_{apop}(u) := \sqrt{\frac{1}{N_d - 1} \sum_{i=1}^{N_d} (P(apoptosis|u) - \bar{P}(apoptosis|u))^2} \quad \forall u \in \mathcal{U} \quad (5)$$

6.4 Implementation

The entirety of the workflow presented here was implemented using the programming language Julia.³² Specifically, we utilize the probabilistic programming library Turing.jl²⁹ to implement our probabilistic model for Bayesian inference. To sample the posterior chain and obtain posterior probability distributions, we use the No U-Turn Sampler (NUTS), a variant of HMC, with an acceptance rate of 0.65. The ODE model evaluations within the probabilistic model are conducted via the DifferentialEquations.jl library.³⁰

The implementation of BOED we propose here exploits several elements of high-performance computing approaches to accelerate the optimization process. First, the implementation of the ODE model was translated into the low-level programming language, Julia, from the rule-based modeling language, BioNetGen.³¹ When performing ODE model simulations at the nominal parameter settings, the BioNetGen implementation requires 0.10 seconds of CPU time. In contrast, solving the ODE model under the same nominal parameter settings using Julia takes only 0.0018 seconds of CPU time. Consequently, our Julia-based model implementation exhibits an impressive 98% reduction in CPU time compared to the BioNetGen implementation. Although these individual execution times may already appear low, the acceleration of individual model evaluations is critically important in the context of Bayesian optimal experimental design. This is because these model evaluations are used in estimating the data likelihood across various parameter values, and as the number of these evaluations increases, the cumulative effect on computational time of Bayesian inference becomes more pronounced. Secondly, we accelerate the computation of each of the 100 posterior estimates per experimental design by using 100 CPU cores in parallel. This means that we can compute 100 posteriors simultaneously, decreasing the time-to-solution over a sequential approach. Thus, we show that the combined utilization of these high-performance computing strategies enhances the efficiency and practical applicability of our proposed Bayesian optimal experimental design framework within the context of a complex PD model. All instances of posterior sampling through NUTS were solved on the Institutional Cluster at the Scientific Data and Computing Center at Brookhaven National Library. Runs were done in parallel using 3 nodes at a time. Each node used consists of 2 CPUs Intel(R) Xeon(R) CPU E5-2695 v4 @ 2.10GHz with 18 cores each.

Funding

This work was supported by the New York Empire State Development Big Data 800 Science Capital Project, the DOE Advanced Scientific Computing Research Applied 801 Mathematics Fellowship, and the Brookhaven Laboratory Directed Research and 802 Development DEDUCE Project. (NMI, KRR, BJY, NMU)

Funding sources include federal funds from the National Cancer Institute, National 793 Institutes of Health, and the Department of Health and Human Services, Leidos Biomedical 794 Research Contract No. 75N91019D00024, Task Order 75N91019F00134 through the 795 Accelerating Therapeutics for Opportunities in Medicine (ATOM) Consortium under 796 CRADA TC02349. (SDM)

Acknowledgements

The authors would like to acknowledge Manasi P. Jogalekar and Morgan E. Diolaiti for providing experimental data related to the IC₅₀ for Talazoparib used in this work.

In addition, we acknowledge the roles of Naomi Ohashi and Eric A. Stahlberg for their project management roles at the Frederick National Laboratory for Cancer Research and ATOM Research Alliance.

Author Contributions

Conceptualization of problem, NMI, SDM, BJY, KR, and NMU; Methodology, NMI, SDM, BJY, KR, and NMU; Implementation, NMI; Analysis, NMI, SDM, BJY, KR, and NMU; Writing – original draft, NMI; Writing – reviewing and editing, NMI, SDM, BJY, KR, and NMU.

Declaration of Interests

SDM is Founder and CEO of BioSystems Strategies, LLC.

NMI, BJY, KR, and NMU declare no competing interests.

References

- ¹ Victor T Sabe, Thandokuhle Ntombela, Lindiwe A Jhamba, Glenn EM Maguire, Thavendran Govender, Tricia Naicker, and Hendrik G Kruger. Current trends in computer aided drug design and a highlight of drugs discovered via computational techniques: A review. *European Journal of Medicinal Chemistry*, 224:113705, 2021.
- ² Rainer Breitling, David Gilbert, Monika Heiner, and Richard Orton. A structured approach for the engineering of biochemical network models, illustrated for signalling pathways. *Briefings in bioinformatics*, 9(5):404–421, 2008.
- ³ William W Chen, Mario Niepel, and Peter K Sorger. Classic and contemporary approaches to modeling biochemical reactions. *Genes & development*, 24(17):1861–1875, 2010.
- ⁴ H Frederik Nijhout, Janet A Best, and Michael C Reed. Systems biology of robustness and homeostatic mechanisms. *Wiley Interdisciplinary Reviews: Systems Biology and Medicine*, 11(3):e1440, 2019.
- ⁵ Sietse Braakman, Pras Pathmanathan, and Helen Moore. Evaluation framework for systems models. *CPT: Pharmacometrics & Systems Pharmacology*, 11(3):264–289, 2022.
- ⁶ Marco Viceconti, Francesco Pappalardo, Blanca Rodriguez, Marc Horner, Jeff Bischoff, and Flora Musuamba Tshinanu. In silico trials: Verification, validation and uncertainty quantification of predictive models used in the regulatory evaluation of biomedical products. *Methods*, 185:120–127, 2021.
- ⁷ Francesco Pappalardo, Giulia Russo, Flora Musuamba Tshinanu, and Marco Viceconti. In silico clinical trials: concepts and early adoptions. *Briefings in bioinformatics*, 20(5):1699–1708, 2019.
- ⁸ Eshan D Mitra and William S Hlavacek. Parameter estimation and uncertainty quantification for systems biology models. *Current opinion in systems biology*, 18:9–18, 2019.
- ⁹ Asbjørn Thode Reenberg, Tobias KS Ritschel, Bernd Dammann, and John Bagterp Jørgensen. High-performance uncertainty quantification in large-scale virtual clinical trials of closed-loop diabetes treatment. In *2022 American Control Conference (ACC)*, pages 1367–1372. IEEE, 2022.
- ¹⁰ Stephen Wu, Panagiotis Angelikopoulos, James L Beck, and Petros Koumoutsakos. Hierarchical stochastic model in bayesian inference for engineering applications: Theoretical implications and efficient approximation. *ASCE-ASME Journal of Risk and Uncertainty in Engineering Systems, Part B: Mechanical Engineering*, 5(1):011006, 2019.
- ¹¹ Jochen Einbeck, Elizabeth A Ainsbury, Rachel Sales, Stephen Barnard, Felix Kaestle, and Manuel Higuera. A statistical framework for radiation dose estimation with uncertainty quantification from the γ -h2ax assay. *PLoS One*, 13(11):e0207464, 2018.
- ¹² Haoyang Zeng and David K Gifford. Quantification of uncertainty in peptide-mhc binding prediction improves high-affinity peptide selection for therapeutic design. *Cell systems*, 9(2):159–166, 2019.
- ¹³ Andreas Raue, Clemens Kreutz, Thomas Maiwald, Julie Bachmann, Marcel Schilling, Ursula Klingmüller, and Jens Timmer. Structural and practical identifiability analysis of partially observed dynamical models by exploiting the profile likelihood. *Bioinformatics*, 25(15):1923–1929, 2009.

- ¹⁴ Oana-Teodora Chis, Alejandro F. Villaverde, Julio R. Banga, and Eva Balsa-Canto. On the relationship between sloppiness and identifiability. *Mathematical Biosciences*, 282:147–161, 2016.
- ¹⁵ A Raue, V Becker, U Klingmüller, and J Timmer. Identifiability and observability analysis for experimental design in nonlinear dynamical models. *Chaos: An Interdisciplinary Journal of Nonlinear Science*, 20(4):045105, 2010.
- ¹⁶ Juliane Liepe, Sarah Filippi, Michał Komorowski, and Michael PH Stumpf. Maximizing the information content of experiments in systems biology. *PLoS computational biology*, 9(1):e1002888, 2013.
- ¹⁷ Samuel Bandara, Johannes P Schlöder, Roland Eils, Hans Georg Bock, and Tobias Meyer. Optimal experimental design for parameter estimation of a cell signaling model. *PLoS computational biology*, 5(11):e1000558, 2009.
- ¹⁸ Olivia Eriksson, Alexandra Jauhiainen, Sara Maad Sasane, Andrei Kramer, Anu G Nair, Carolina Sartorius, and Jeanette Hellgren Kotaleski. Uncertainty quantification, propagation and characterization by bayesian analysis combined with global sensitivity analysis applied to dynamical intracellular pathway models. *Bioinformatics*, 35(2):284–292, 2019.
- ¹⁹ Antony M Overstall, David C Woods, and Ben M Parker. Bayesian optimal design for ordinary differential equation models with application in biological science. *Journal of the American Statistical Association*, 2019.
- ²⁰ Tom Rainforth, Adam Foster, Desi R Ivanova, and Freddie Bickford Smith. Modern bayesian experimental design. *arXiv preprint arXiv:2302.14545*, 2023.
- ²¹ Roozbeh Dehghannasiri, Byung-Jun Yoon, and Edward R Dougherty. Optimal experimental design for gene regulatory networks in the presence of uncertainty. *IEEE/ACM Transactions on Computational Biology and Bioinformatics*, 12(4):938–950, 2014.
- ²² Youngjoon Hong, Bongsuk Kwon, and Byung-Jun Yoon. Optimal experimental design for uncertain systems based on coupled differential equations. *IEEE Access*, 9:53804–53810, 2021.
- ²³ Byung-Jun Yoon, Xiaoning Qian, and Edward R Dougherty. Quantifying the objective cost of uncertainty in complex dynamical systems. *IEEE Transactions on Signal Processing*, 61(9):2256–2266, 2013.
- ²⁴ Byung-Jun Yoon, Xiaoning Qian, and Edward R Dougherty. Quantifying the multi-objective cost of uncertainty. *IEEE Access*, 9:80351–80359, 2021.
- ²⁵ Dennis V Lindley. On a measure of the information provided by an experiment. *The Annals of Mathematical Statistics*, 27(4):986–1005, 1956.
- ²⁶ Xun Huan and Youssef M Marzouk. Simulation-based optimal bayesian experimental design for nonlinear systems. *Journal of Computational Physics*, 232(1):288–317, 2013.
- ²⁷ Susan D. Mertins, Natalie M. Isenberg, Kristofer-Roy Reyes, Byung-Jun Yoon, Nathan Urban, Manasi P. Jogalekar, Morgan E. Diolaiti, M. Ryan Weil, and Eric A. Stahlberg. Pharmacodynamic model of parp1 inhibition and global sensitivity analyses can lead to cancer biomarker discovery. *bioRxiv*, 2023.
- ²⁸ Leo L Duan, Alexander L Young, Akihiko Nishimura, and David B Dunson. Bayesian constraint relaxation. *Biometrika*, 107(1):191–204, 2020.
- ²⁹ Hong Ge, Kai Xu, and Zoubin Ghahramani. Turing: a language for flexible probabilistic inference. In *International conference on artificial intelligence and statistics*, pages 1682–1690. PMLR, 2018.
- ³⁰ Christopher Rackauckas and Qing Nie. Differentialequations. jl—a performant and feature-rich ecosystem for solving differential equations in julia. *Journal of open research software*, 5(1), 2017.
- ³¹ James R Faeder, Michael L Blinov, and William S Hlavacek. Rule-based modeling of biochemical systems with bionetgen. *Systems biology*, pages 113–167, 2009.
- ³² Jeff Bezanson, Stefan Karpinski, Viral B Shah, and Alan Edelman. Julia: A fast dynamic language for technical computing. *arXiv preprint arXiv:1209.5145*, 2012.

Supplemental Information

7 Uncertain Parameter Information

Prior information for the uncertain parameters considered in this study was first elicited from expert understanding of the system and relevant sources and is compiled in Table 1. This table shows the model parameters, their nominal values, and estimated 90% confidence interval lower and upper limits.

Parameter	Units	Nominal Value	Lower Confidence Bound	Upper Confidence Bound
s_1	mol s ⁻¹	1×10^{-2}	4.5×10^{-3}	2.2×10^{-2}
s_2	mol s ⁻¹	3×10^{-2}	1.3×10^{-2}	6.7×10^{-2}
s_3	mol s ⁻¹	2×10^1	4.2×10^{-1}	9.42×10^2
s_4	mol s ⁻¹	2×10^{-1}	4.5×10^{-2}	8.9×10^{-1}
d_1	s ⁻¹	1×10^{-3}	4.5×10^{-4}	2.2×10^{-3}
d_2	s ⁻¹	1×10^{-4}	2.0×10^{-5}	5.1×10^{-4}
d_3	s ⁻¹	2×10^{-4}	3.9×10^{-5}	1.0×10^{-3}
M	-	100,000	90,453	110,554
b_1	mol ⁻¹ s ⁻¹	3×10^{-5}	3.9×10^{-6}	2.3×10^{-4}
a_1	mol ⁻¹ s ⁻¹	2×10^{-10}	4.14×10^{-11}	9.66×10^{-10}
a_2	mol ⁻¹ s ⁻¹	1×10^{-12}	6.55×10^{-13}	1.53×10^{-12}

Table 1: Table of uncertain parameters and 90% confidence limits for the *PARP1* inhibitor ODE model. All prior probability distributions are assumed to be log-normal to prohibit negative rate parameter values.

Derived prior probability distributions for each uncertain parameter considered in the model are described in Table 2. All priors are defined as Log-Normal probability distributions. For all parameters, the nominal value was taken as the mean. Because the lower and upper bounds on the uncertain parameters are not centered at the nominal value, the width of this CI range was used to compute the geometric distance from the nominal to new lower and upper bounds in log-space.

Parameter	Log Mean	Log Std
s_1	-4.61	0.49
s_2	-3.51	0.49
s_3	3.00	2.34
s_4	-1.61	0.91
d_1	-6.91	0.49
d_2	-9.21	1.00
d_3	-8.52	1.00
M	11.51	0.06
b_1	-10.41	1.24
a_1	-22.33	0.96
a_2	-27.63	0.26

Table 2: Table of distributional information (mean, standard deviation) for Log-Normal priors on all uncertain parameters considered in this work.

8 Experimental Designs

The list of measurable species considered as potential “experimental designs” in the present study are shown in Table 3.

Species Symbol	Definition
mRNA-Bax	Messenger mRNA for Bax
Bad-Bcl-xL	Bad bound to Bcl-xL
Casp-pro	Inactive caspase
Bax-Bcl-xL	Bax bound to Bcl-xL
Casp-act	Activated caspase

Table 3: Table of measurable species in the *PARP1* inhibited ODE model. As in,²⁷ all initial values for these species is 0. The ODE model computes concentrations in dimensionless units [*Molec.*] representing molecules-per-cell.

Measured Protein	σ_{apop}									
	$IC_{50} =$	0.001	0.01	0.03	0.1	0.3	1.0	3.0	10	100
mRNA-Bax		0.0	0.00446	0.0077	0.0128*	0.0190*	0.0261*	0.0231*	0.0190*	0.0
Bad-Bcl-xL		0.0	0.00446	0.0076	0.0144	0.0199	0.0277	0.0271	0.0195	0.0
Casp-pro		0.0	0.0119	0.0205	0.0355	0.0413	0.0494	0.0435	0.0273	0.0
Bax-Bcl-xL		0.0	0.0041	0.0095	0.0342	0.0353	0.0309	0.0283	0.0211	0.0
Casp-act		0.0	0.0034*	0.0074*	0.0158	0.0289	0.0421	0.0418	0.0277	0.0

Table 4: Table of σ_{apop} results for each measureable protein in the *PARP1*-inhibited cell apoptosis model. The minimum value in each column is denoted with an *.

Measured Species	$\sigma_{IC_{50}}$					
	Threshold=	0.5	0.6	0.7	0.8	0.9
mRNA-Bax		0.170*	0.113*	0.075*	0.047*	0.023*
Bad-Bcl-xL		0.179	0.117	0.078	0.049	0.026
Casp-pro		0.327	0.226	0.153	0.095	0.047
Bax-Bcl-xL		0.208	0.147	0.102	0.066	0.033
Casp-act		0.390	0.278	0.179	0.109	0.053

Table 5: Table of $\sigma_{IC_{50}}$ results for each measureable protein in the *PARP1*-inhibited cell apoptosis model. The minimum value in each column is denoted with an *.

9 Tabulated Objective Data

$\sigma_{apop}(0.01)$	$\sigma_{IC_{50}}(0.9)$	$w_1 = 0.01$	$w_1 = 0.1$
$\xi^* = \text{Casp-act}$	$\xi^* = \text{mRNA-Bax}$	$\xi^* = \text{Casp-act}$	$\xi^* = \text{mRNA-Bax}$

Table 6: Table of optimal experimental designs, ξ^* for each objective considered in the present study.

10 Posterior Chain Summary Statistics

Each table in this section presents summary statistics for uncertain parameter values and effective sample size for each uncertain parameter inferred in Bayesian inference against a specific species measurement. Averages are computed over 100 synthetic experimental datum for that protein generated according to the procedure described in the STAR Methods. An additional table is provided per each species to list the min, max, and average chain size from all 100 posteriors used in obtaining these statistics.

mRNA-Bax

Parameter	Mean Value	Average ESS
s_1	1.01×10^{-2}	561
s_2	3.70×10^{-2}	565
s_3	141.3	566
s_4	2.80×10^{-1}	563
d_1	1.14×10^{-3}	560
d_2	1.33×10^{-4}	550
d_3	2.74×10^{-4}	569
M	100,276	565
b_1	6.82×10^{-5}	566
a_1	3.27×10^{-10}	562
a_2	1.03×10^{-12}	549

Table 7: Average expected parameter values and effective sample size from filtered chains for posteriors obtained via mRNA-Bax data.

Min	Max	Average
348	690	594

Table 8: Chain length statistics (min, max, and average) after sample rejection for mRNA-Bax.

Bad-Bcl-xL

Parameter	Mean Value	Average ESS
s_1	1.02×10^{-2}	549
s_2	3.74×10^{-2}	541
s_3	136.875	542
s_4	2.82×10^{-1}	540
d_1	1.12×10^{-3}	545
d_2	1.36×10^{-4}	531
d_3	2.79×10^{-4}	539
M	101,239	554
b_1	7.09×10^{-5}	525
a_1	3.30×10^{-10}	550
a_2	1.04×10^{-12}	557

Table 9: Average expected parameter values and effective sample size from filtered chains for posteriors obtained via Bad-Bcl-xL data.

Min	Max	Average
111	715	606

Table 10: Chain length statistics (min, max, and average) after sample rejection for Bad-Bcl-xL.

Casp-pro

Parameter	Mean Value	Average ESS
s_1	7.91×10^{-3}	226
s_2	2.84×10^{-2}	238
s_3	34.15	195
s_4	2.4×10^{-1}	235
d_1	7.93×10^{-4}	233
d_2	8.19×10^{-5}	228
d_3	3.07×10^{-4}	195
M	75,191	224
b_1	4.90×10^{-5}	228
a_1	2.47×10^{-10}	219
a_2	7.50×10^{-13}	220

Table 11: Average expected parameter values and effective sample size from filtered chains for posteriors obtained via Casp-pro data.

Min	Max	Average
192	1343	648

Table 12: Chain length statistics (min, max, and average) after sample rejection for Casp-pro.

Bax-Bcl-xL

Parameter	Mean Value	Average ESS
s_1	1.02×10^{-2}	623
s_2	3.73×10^{-2}	620
s_3	129.6	616
s_4	2.83×10^{-1}	614
d_1	1.10×10^{-3}	615
d_2	1.32×10^{-4}	606
d_3	2.82×10^{-4}	610
M	100,209	610
b_1	7.48×10^{-5}	606
a_1	3.25×10^{-10}	607
a_2	1.03×10^{-12}	614

Table 13: Average expected parameter values and effective sample size from filtered chains for posteriors obtained via Bax-Bcl-xL data.

Min	Max	Average
107	1115	812

Table 14: Chain length statistics (min, max, and average) after sample rejection for Bax-Bcl-xL.

Casp-act

Parameter	Mean Value	Average ESS
s_1	9.00×10^{-3}	249
s_2	3.31×10^{-2}	250
s_3	110.6	243
s_4	2.11×10^{-1}	249
d_1	1.05×10^{-3}	245
d_2	1.39×10^{-4}	247
d_3	1.80×10^{-4}	242
M	91,317	259
b_1	6.26×10^{-5}	249
a_1	2.83×10^{-10}	247
a_2	9.51×10^{-13}	253

Table 15: Average expected parameter values and effective sample size from filtered chains for posteriors obtained via Casp-act data.

Min	Max	Average
265	1568	1180

Table 16: Chain length statistics (min, max, and average) after sample rejection for Casp-act.

11 Prior predictive distributions

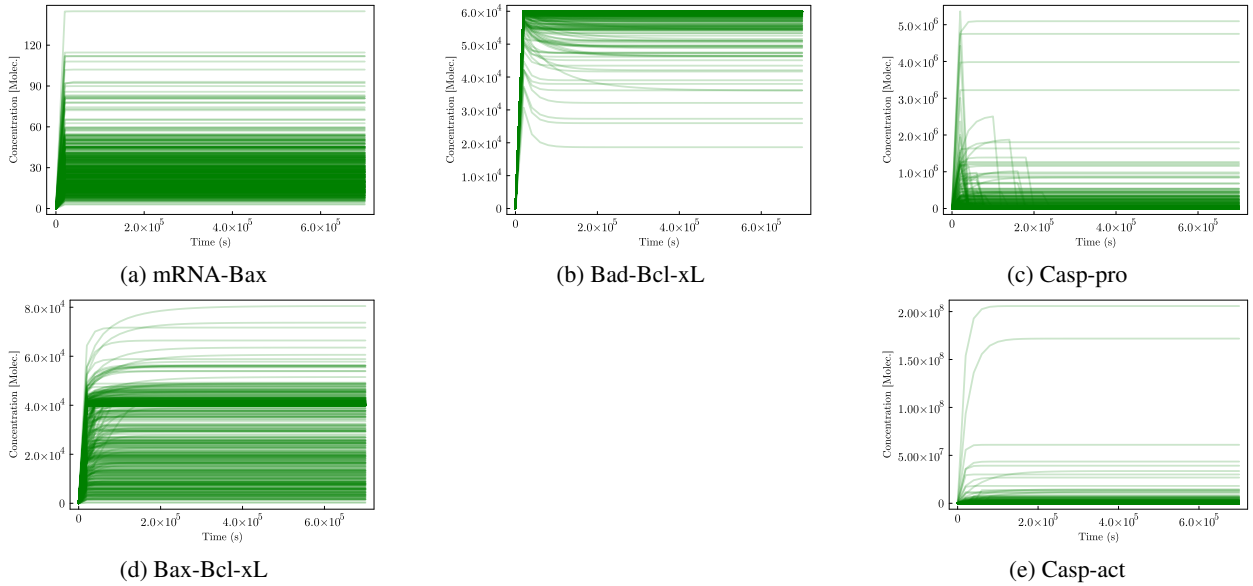


Figure 8: Prior predictive plots from 500 simulations sampled randomly from the prior distributions of the uncertain parameters and run through the forward ODE model to create concentration profile distributions. Units of concentration are in molecules-per-cell.

12 Mathematical Model

This section contains the full system of differential equations that define the *PARP1*-inhibited cell apoptosis model as presented in.²⁷ In the notation in Equation 6, \dot{x}_i refers to the time-varying rate of change of species i , where $i = \{1, \dots, 23\}$, x_i is the species concentration in units of molec/cell, and p_i , $i = \{1, \dots, 27\}$ are the ODE parameters related to rates. See Tables 17 and 18 for a mapping from x_i and p_i notation to biological symbols and values. This mathematical model was generated from the rule-based modeling software, BioNetGen, using the previously published PARP1-inhibited cell apoptosis model in.²⁷

$$\begin{aligned}
 \dot{x}_1 &= -p_{12}x_2x_1 - p_{12}x_6x_1 + p_{16}x_{11} + p_{16}x_{12} + p_{24}x_{10}x_{12} - p_{25}x_{19}x_1 \\
 \dot{x}_2 &= -p_{12}x_2x_1 + p_{16}x_{11} \\
 \dot{x}_3 &= -p_{10}x_3x_4 - p_9x_{14}x_3 + p_{14}x_{15} + p_{42}x_{15} + p_{13}x_{20} + p_6x_{20} \\
 \dot{x}_4 &= -p_{10}x_3x_4 - p_{41}x_4 + p_{14}x_{15} + p_{18}x_{16} + p_{18}x_{21} \\
 \dot{x}_5 &= -p_{11}x_{16}x_5 + p_{15}x_{21} + p_{18}x_{21} \\
 \dot{x}_6 &= -p_{12}x_6x_1 + p_{16}x_{12} \\
 \dot{x}_7 &= -p_{21}x_{12}x_7 + p_{22}x_{18} + p_{26}x_{18}x_8 \\
 \dot{x}_8 &= -p_{26}x_{18}x_8 + p_{27}x_9x_{23} \\
 \dot{x}_9 &= 0 \\
 \dot{x}_{10} &= -p_{24}x_{10}x_{12} + p_{25}x_{19}x_1 \\
 \dot{x}_{11} &= +p_{12}x_2x_1 - p_{16}x_{11} \\
 \dot{x}_{12} &= +p_{12}x_6x_1 - p_{16}x_{12} - p_{21}x_{12}x_7 - p_{24}x_{10}x_{12} + p_{22}x_{18} + p_{26}x_{18}x_8 + p_{25}x_{19}x_1 \\
 \dot{x}_{13} &= +p_1 + p_{39} - p_5x_{13} \\
 \dot{x}_{14} &= +p_{40} - p_6x_{14} - p_9x_{14}x_3 + p_{13}x_{20} \\
 \dot{x}_{15} &= +p_{10}x_3x_4 - p_{14}x_{15} - p_{42}x_{15} \\
 \dot{x}_{16} &= +p_{41}x_4 - p_{18}x_{16} - p_{11}x_{16}x_5 + p_{42}x_{15} + p_{15}x_{21} \\
 \dot{x}_{17} &= +p_3 - p_7x_{17} - p_{43}x_{17} \\
 \dot{x}_{18} &= +p_{21}x_{12}x_7 - p_{22}x_{18} - p_{26}x_{18}x_8 \\
 \dot{x}_{19} &= +p_{24}x_{10}x_{12} - p_{25}x_{19}x_1 \\
 \dot{x}_{20} &= +p_9x_{14}x_3 - p_{13}x_{20} - p_6x_{20} \\
 \dot{x}_{21} &= +p_{11}x_{16}x_5 - p_{15}x_{21} - p_{18}x_{21} \\
 \dot{x}_{22} &= +p_{43}x_{17} - p_7x_{22} \\
 \dot{x}_{23} &= +p_{26}x_{18}x_8 - p_{27}x_9x_{23}
 \end{aligned} \tag{6}$$

Symbol	Species	Description	Initial Values
x_1	DNADSB	DNA double strand break	1.74×10^5
x_2	p53	p53 transcription factor	8.5×10^4
x_3	Bcl-xL	Anti-apoptotic factor	1×10^5
x_4	Bad	Pro-apoptotic factor	6×10^4
x_5	Scaffold 14-3-3	Scaffold 14-3-3	2×10^5
x_6	PARP	Poly(ADP-ribose) polymerase	1.07×10^5
x_7	NAD	Nicotinamide adenosine deoxyribose	1.07×10^6
x_8	XRCC1(Glu~uPAR)	PARP substrate XRCC1 unPARylated	1.07×10^5
x_9	PARG	Poly(ADP-ribose) glycohydrazase	1.07×10^4
x_{10}	Inhibitor	Generic PARP inhibitor	0.005083
x_{11}	DNADSB-p53	p53 bound to DNA double strand break	0
x_{12}	DNADSB-PARP	PARP bound to DNA double strand break	0
x_{13}	mRNA-Bax	Messenger RNA for Bax	0
x_{14}	Bax	Pro-apoptotic factor	0
x_{15}	Bad-Bcl-xL	Bad bound to Bcl-xL	0
x_{16}	Bad(S75 S99~PP,b)	Phosphorylated Bad	0
x_{17}	Casp-pro	Inactive caspase	0
x_{18}	DNADSB-NAD-PARP	NAD bound to PARP active site while PARP bound to DNA	0
x_{19}	Inh-PARP	Inhibitor bound to PARP	0
x_{20}	Bax-Bcl-xL	Bax bound to Bcl-xL	0
x_{21}	Bad-Scaffold 14-3-3	Bad bound to Scaffold 14-3-3	0
x_{22}	Casp-act	Active caspase	0
x_{23}	XRCC1(Glu~Par)	PARP substrate XRCC1 PARylated	0

Table 17: Mapping between symbol and species name in the ODE model in Equation 6.

Symbol	Species	Nominal Value
p_1	s_1	0.01
p_2	s_2	0.03
p_3	s_3	20
p_4	s_4	0.2
p_5	d_1	0.001
p_6	d_1	0.0001
p_7	d_1	0.002
p_8	M	10,000
p_9	b_1	3×10^{-5}
p_{10}	b_2	0.003
p_{11}	b_3	0.003
p_{12}	b_4	3×10^{-5}
p_{13}	u_1	0.0001
p_{14}	u_2	0.0001
p_{15}	u_3	0.0001
p_{16}	u_4	0.0001
p_{17}	p_1	3×10^{-10}
p_{18}	q_1	3×10^{-5}
p_{19}	a_1	2×10^{-10}
p_{20}	a_2	1×10^{-12}
p_{21}	kf_1	0.001
p_{22}	kr_1	3.79
p_{23}	IC_{50}	N/A
p_{24}	kf_2	0.001
p_{25}	kr_2	0.00379
p_{26}	$kcat_1$	1
p_{27}	$kcat_2$	1

Table 18: Mapping between symbol and parameter name in the ODE model in Equation 6. There is no nominal value specified for $p_{23}=IC_{50}$ because it is a decision variable and its value is subject to change within our studies.